Minerals Engineering 146 (2020) 106137

Contents lists available at ScienceDirect

Minerals Engineering

journal homepage: www.elsevier.com/locate/mineng

Study of collisions between particles and unloaded bubbles with point-particle model embedded in the direct numerical simulation of turbulent flows

Dongdong Wan[a], Xuan Yi[b], Lian-Ping Wang[c,d], Xun Sun[a], Songying Chen[a], Guichao Wang[a,e,*]

[a] Key Laboratory of High-efficiency and Clean Mechanical Manufacture, School of Mechanical Engineering, Shandong University, Jinan 250061, PR China
[b] International Economic & Technical Cooperation and Exchange Center, Ministry of Water Resources, Beijing 100038, PR China
[c] Department of Mechanics and Aerospace Engineering, Southern University of Science and Technology, Shenzhen 518055, PR China
[d] Department of Mechanical Engineering, 126 Spencer Laboratory, University of Delaware, Newark, DE 19716-3140, USA
[e] SUSTech Academy for Advanced Interdisciplinary Studies, Southern University of Science and Technology, Shenzhen 518055, PR China

ARTICLE INFO

Keywords:
DNS
Particle-bubble collision
Turbulence
Point-particle model

ABSTRACT

Simulations of a particle-bubble collision system composed of monosized spherical solid particles and air bubbles in a quiescent liquid and homogeneous isotropic turbulence have been performed using the pseudo-spectral method for the fluid flow and Lagrangian tracking for particles and bubbles. Particle-bubble collisions in a quiescent liquid were first simulated and compared to the existing theoretical models of particle-bubble collisions. Both numerical results and theoretical models indicate that decreasing bubble size and increasing particle size can increase the particle-bubble collision efficiency. A DNS model for studying the effect of turbulence on the collisions between particles and unloaded bubbles was then developed. A nonuniform time-dependent stochastic forcing scheme was implemented to maintain turbulence intensity at targeted levels. A statistical analysis of a group of particles and bubbles in the forced turbulent flow was performed to probe the mechanism of particle-bubble collision in a turbulent flow. A simplifying assumption (motivated purely by computational limitations) has been made that bubbles and particles can be randomly relocated during the simulation, unlike what happens in reality, but the size of the effect that this simplifying assumption will have on our results is unknown. Reductions in particle-bubble collisions due to preferential concentrations of particles and bubbles in different flow regions were not found. Comparing respectively the contributions of radial relative velocity and radial distribution function to the collision kernel, the contribution of radial distribution function could be neglected because the radial relative velocity increases by about 1900% (from 1.55 cm/s to 28.87 cm/s) while the radial distribution function decreases by only 33% (from 1.33 to 1.00). Collisions between particles and bubbles increased with turbulent dissipation rate primarily due to the fact that radial relative velocities between particles and bubbles increased with the flow dissipation rate.

1. Introduction

Particle-bubble collisions play an important role in froth flotation, which is commonly encountered in many industrial processes including deinking of waste paper, water treatment, mineral beneficiation and petrochemical processes. The essence of flotation lies in using bubbles to capture particles based on their surface hydrophobicity differences. After collisions between particles and bubbles, hydrophobic particles are more likely to attach to a bubble interface due to strong adhesion force leaving hydrophilic particles in the pulp phase. Flotation model can be considered as a first order chemical kinetic process relating the rate of particle attachment to particle concentration (Ahmed and Jameson, 1989; Klassen and Mokrousov, 1963; Sutherland, 1948). Most researchers consider the rate of particle capture in a batch flotation process as:

$$\frac{dC}{dt} = -\mathscr{K}C \tag{1}$$

where C is the particle concentration in the pulp in units of numbers/volume and $\mathscr{K}$ is the flotation rate constant. It is noted that Eq. (1) only applies to model the removal of particles in a batch process. In a

* Corresponding author at: Key Laboratory of High-efficiency and Clean Mechanical Manufacture, School of Mechanical Engineering, Shandong University, Jinan 250061, PR China.
E-mail address: guichao.wang@uon.edu.au (G. Wang).

https://doi.org/10.1016/j.mineng.2019.106137
Received 29 January 2019; Received in revised form 13 November 2019; Accepted 22 November 2019
Available online 29 November 2019
0892-6875/

Nomenclature

Symbol	Meaning, Unit
a	the ratio of particle diameter to bubble diameter, -
C	particle concentration, $1/m^3$
c_1	coefficients related to the Reynolds number of bubbles, -
c_2	coefficients related to the Reynolds number of bubbles, -
$\boldsymbol{d}^{(mj)}$	the distance between the j^{th} particle at position $\boldsymbol{Y}_{\mathbf{p}}^{(j)}$ and the m^{th} particle at position $\boldsymbol{Y}_{\mathbf{p}}^{(m)}$, cm
d_b	bubble diameter, μm
d_p	particle diameter, μm
E_c	collision efficiency, –
$E_{c,i}$	interceptional collision efficiency, –
$E_{c,in}$	inertial collision efficiency, –
$E_{c,g}$	gravitational collision efficiency, –
$f(Re_\alpha)$	non-linear drag coefficient, –
$\overrightarrow{f}$	external force, N
g_i	the gravity force, N
$\overline{g}(R_c)$	radial distribution function, –
h	depth of flotation cells, m
k_i	the discretized wavenumber in i direction, pseudo-spectral unit
k_F	forcing radius, pseudo-spectral unit
$\mathscr{K}$	flotation rate constant, 1/s
$N_{\alpha c}(t^{n-1} \rightarrow t^n)$	the number of collision events happening in the time interval $t^{n-1} \rightarrow t^n$ for particle-particle or bubble-bubble collisions, $1/(s{\cdot}cm^3)$
$N_{pbc}(t^{n-1} \rightarrow t^n)$	the number of collision events happening in the time interval $t^{n-1} \rightarrow t^n$ for particle-bubble collisions, $1/(s{\cdot}cm^3)$
$\mathscr{N}_{\alpha\alpha}$	The number of collision events in unit time and unit space, for the particle-particle collision or bubble-bubble collision, $1/(s{\cdot}cm^3)$
$N_{pairs}(t^{n-1} \rightarrow t^n)$	the number of pairs that can be found in the shell, $1/(s{\cdot}cm^3)$
$\mathscr{N}_{pb}$	the number of collision events between particles and bubbles in unit time and unit space, $1/(s{\cdot}cm^3)$
N	number of discretized nodes in each direction of the computation domain, 1
N_p	total number of particles, 1
N_b	total number of bubbles, 1
n_α	the number density of N_p particles or N_b bubbles with Ω being the volume of the domain, $1/cm^3$
n_p	number density of particles, $1/cm^3$
n_b	number density of bubbles, $1/cm^3$
p	pressure, Pa
$P_{collection}$	probability that a particle can be collected from the pulp phase by rising bubbles, –
P_c	collision probability, –
P_a	attachment probability, –
P_d	probability of particle detachment from the bubble, –
Q	gas volumetric flowrate, m^3/s
$\mathscr{R}$	flotation recovery, –
R_T	truncation radius, μm
R_c	the collision radius, μm
Re	Reynolds number, dimensionless
Re_α	particle Reynolds number, dimensionless
$r_p^{(j)}$	the j^{th} particle at position $\boldsymbol{Y}_{\mathbf{p}}^{(j)}$ with radius, μm
$\boldsymbol{r}^{(j)}$	the distance between the j^{th} particle at position $\boldsymbol{Y}_{\mathbf{p}}^{(j)}$ and the j^{th} particle at position $\boldsymbol{Y}_{\mathbf{p}}^{(j)}$, cm
r_α	particle or bubble radius, μm
r_b	bubble radius, μm
r_p	particle radius, μm
$St_{Schulze}$	the Stokes number defined by Schulze, –
Δt	time step size, ms
T_F	forcing timescale, pseudo-spectral unit
$\overrightarrow{U}$	fluid velocity, cm/s
$\widetilde{\boldsymbol{u}}^{(j)}(\boldsymbol{Y}_{\boldsymbol{p}}^{(j)})$	the disturbance field at the location of the j^{th} particle, cm/s
$\boldsymbol{u}_s$	the Stokes disturbance flow, cm/s
U_i	fluid velocity at the location of the particles, cm/s
$\widetilde{u}_i$	the disturbance flow velocities from surrounding particles, cm/s
$\overrightarrow{u}$	fluid velocity, cm/s
$\overrightarrow{V}$	particle velocity, cm/s
$\boldsymbol{V}^{(j)}$	velocity of the j^{th} particle at position $\boldsymbol{Y}_{\mathbf{p}}^{(j)}$, cm/s
V_i	particle velocity, cm/s
V_c	effective volume of the cell, m^3
v_p	particle settling velocity, cm/s
v_b	bubble rising velocity, cm/s
V_{shell}	volume of the shell used to find colliding pairs, cm^3
$\overline{\lvert w_r \rvert}(R_c)$	radial relative velocity, cm/s
$\boldsymbol{Y}_{\mathbf{p}}^{(j)}$	position of the j^{th} particle, cm

Greek symbols

β_α	a coefficient with ρ_f being the fluid density, –
$\Gamma_{\alpha\alpha}$	collsion kernel for self-collisions, cm^3/s
Γ_{pb}	collsion kernel between particles and bubbles, cm^3/s
$\Gamma_{pb}^D(t^n)$	The dynamic kernels, cm^3/s
$\Gamma^K(t^n)$	Kinematic kernels, cm^3/s
δ	thickness of the shell used to find colliding pairs, cm
η_K	kolmogorov length scale of the turbulence, μm
μ_f	dynamic viscosity of the fluid, Pa·s
ν_f	kinematic viscosity of the fluid, cm^2/s
ρ_b	bubble density, g/cm^3
ρ_p	particle density, g/cm^3
σ_F	forcing amplitude, pseudo-spectral unit
τ_α	response time of particles or bubbles, ms
τ_b	response time of bubbles, ms
τ_K	kolmogorov time scale of the turbulence, ms
τ_p	response time of particles, ms
τ	residence time inside the flotation cell, s
φ_c	critical angle of the grazing trajectory, rad
ψ_g	the value of the stream function which characterizes the grazing trajectory, 1/(s·cm)
Ω	volume of the computational domain, cm^3
$\overrightarrow{\omega}$	vorticity, 1/s

continuous flow flotation cell the inlet and outlet concentrations do not change with time (i.e. steady state), so that Eq. (1) does not apply to the cell as a whole. For continuous flow flotation, the recovery $\mathscr{R}$ can be calculated as:

$$\mathscr{R} = \frac{\mathscr{K}\tau}{1 + \mathscr{K}\tau} \tag{2}$$

where τ is the residence time inside the flotation cell. Throughout modelling endeavour, attention has been paid to the calculation of rate constant $\mathscr{K}$. The critical parameter here is the rate constant $\mathscr{K}$, which in fact is not in any sense a constant. It is a proportionality factor that can be correlated to a particular set of conditions. Therefore, the rate constant is typically expressed as a function of physical parameters of the system (Deglon et al., 1999; Heiskanen, 2000; Jameson et al., 1977; Morris, 1952). It can be written as:

$$\mathscr{K} = \frac{3QhP_{\text{collection}}}{2d_b V_c} \tag{3}$$

where Q is the gas volumetric flowrate, h is the depth of the cell, d_b is the mean bubble diameter, V_c is the effective volume of the cell, $P_{\text{collection}}$ is the probability that a particle can be collected from the pulp phase by rising bubbles. The rate constant is dependent on particle and bubble size. The particle collection process is usually decomposed into three successive steps: collision between particle and bubble; particle attachment to the bubble and particle detachment from the bubble. Therefore, the probability of a particle to be collected is:

$$P_{\text{collection}} = P_c P_a (1 - P_d) \tag{4}$$

where P_c is collision probability, P_a is attachment probability and P_d is the probability of particle detachment from the bubble. It is clear that the collision process, attachment process and detachment process should be each individually modelled properly in order to model the kinetics of the flotation process successfully and to predict the product recovery from limited known input variables. To avoid complexities of particle-bubble interactions in the froth phase for which models are really scarce, and require further research, this work is restrained to the discussion of particle-bubble collision process in the pulp phase only. Particle-bubble collision phenomenon is the key to the success of flotation process, which is facilitated by the local hydrodynamics in the vicinity of a probable particle-bubble collision pair (Wang et al., 2018).

The particle-bubble collision process has been widely investigated and reported. Critical literature reviews on collision models have been presented (Dai et al., 2000; Hassanzadeh et al., 2018; Meyer and Deglon, 2011; Nguyen et al., 2016; Schulze et al., 1989). A brief introduction of particle-bubble collision is made to provide an overview of the development of models of particle-bubble collision. Sutherland (1948) gave a first collision model (as formulated by Formula (5)) for a particle-bubble system based on the assumption that the inertia of particles can be neglected (i.e. particles need to be much smaller than bubbles) and particles follow the streamlines of fluid. The collision efficiency can be calculated from the streamlines of fluid considering potential flow around the bubble surface. The collision radius R_c, defined from a critical streamline of the grazing trajectory of a particle around a bubble is shown in Fig. 1. Particles inside the collision radius are considered to collide with the bubble. Therefore, the collision efficiency E_c is determined by the ratio of the cross-sectional area of the collision radius to the projected area of the bubble. It is:

$$E_c = 3d_p/d_b \tag{5}$$

Gaudin (1957) considered the liquid flow around a bubble in the flotation process to be Stokes flow. On the same assumption of neglecting the inertia of particles as Sutherland, the collision efficiency can be described as:

$$E_c = \frac{3}{2}(d_p/d_b)^2 \tag{6}$$

Yoon and Luttrell (1989) considered different flow conditions around the bubble surface and gave the same equations as the Gaudin collision model in the Stokes flow condition (at very low Reynolds number) and as the Sutherland model in the potential flow condition (at very high Reynolds number). As for the intermediate flow condition specifically, the collision efficiency is:

$$E_c = (d_p/d_b)^2\left(\frac{3}{2} + \frac{4Re^{0.72}}{15}\right) \tag{7}$$

Flint and Howarth (1971) related the particle settling velocity v_p and the bubble rising velocity v_b and gave the collision efficiency as:

$$E_c = v_p/(v_p + v_b) \tag{8}$$

Schulze (1989) considered the particle-bubble collision as a result of interceptional, gravitational and inertial effects. The overall particle-bubble collision efficiency was assumed to be the sum of individual collision efficiencies. The interceptional collision efficiency is:

$$E_{c,i} = \frac{v_b}{v_p + v_b} 2\psi_c \tag{9}$$

where $\psi_c = \psi_g r_b^2/v_b$, ψ_g is the value of the stream function which characterizes the grazing trajectory, r_b is the radius of bubbles. And the gravitational collision efficiency is:

$$E_{c,g} = \frac{v_p}{v_p + v_b}(1 + a)^2 \sin^2\varphi_c \tag{10}$$

where $a = d_p/d_b$ and φ_c is the critical angle of the grazing trajectory. And the inertial collision efficiency is:

$$E_{c,in} = \frac{v_b}{v_p + v_b}(1 + a)^2\left(\frac{St_{\text{Schulze}}}{St_{\text{Schulze}} + c_1}\right)^{c_2} \tag{11}$$

where c_1 and c_2 are coefficients related to the Reynolds number of bubbles, $St_{\text{Schulze}} = \rho_p d_p^2 v_b/(9\mu_f d_b)$ is the Stokes number defined by Schulze in his paper with ρ_p being the particle density and μ_f being the dynamic viscosity of the fluid. And the overall collision efficiency is:

$$E_c = E_{c,i} + E_{c,g} + E_{c,in}\left[1 - \frac{E_{c,i}}{(1 + a)^2}\right] \tag{12}$$

It should be noted that collision models provided by Schulze et al. (1989) are representatives of different mechanisms and other researchers provide collision models of different forms. It was after the first collision model given by Sutherland (1948) that the concept of particle-bubble collision has been widely accepted. The analysis of modeling the collision efficiency has generally assumed quiescent environment as turbulent flows would make the analysis intractable. The fundamental studies attempting to model the particle-bubble collision efficiency are generally based on the assumption that bubbles rise and particles settle in a quiescent environment. Existing theories of the particle-bubble collision are either of empirical nature or do not account for the effect of turbulent liquid flows. There is little experimental work on the direct observation of the collisions between particles and bubbles in turbulent flows, due to the complexities embedded in the subsequent steps of particle attachment and detachment after a particle collides with a bubble.

Single bubble flotation experiments were designed to validate models of particle-bubble collision (Dai et al., 1998; Nutt et al., 1963). Single bubbles rose in the quiescent slurry and particles were considered to attach to the surface of bubbles once they collided with bubbles. Attachment efficiency and stability efficiency (the probability that detachment would not occur) were considered to be equal to one, and the particle-bubble collision efficiency could be represented by particle collection efficiency. A direct method was designed to look at the particle-bubble collision process using a high-speed camera

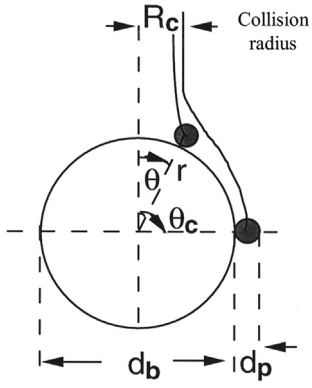

Fig. 1. A schematic representation of the grazing trajectory of a particle with diameter d_p around a bubble in a quiescent liquid (Dai et al., 2000).

(Brabcová et al., 2015; Nguyen Van and Kmeť, 1992; Verrelli et al., 2014, 2011; Wang et al., 2003). A direct observation of the trajectories of falling particles around a stationary bubble was used to determine particle-bubble collisions. It should be mentioned that these experimental studies are limited to the study of particle-bubble collision in a quiescent liquid. While this phenomenon is close to the situation inside a flotation column where bubbles rise and particles settle in a "non-violent" flow environment, more and more industrial applications have applied strong turbulent flow to enhance particle-bubble collisions.

Due to the difficulties of experimental studies of particle-bubble collision in a turbulent flow field, researchers have used computational fluid dynamics for detailed modeling of particle-bubble collisions (Wang et al., 2018). Liu and Schwarz (2009a, b) studied particle-bubble collision efficiency in a turbulent flow. An integrated CFD-based scheme for the prediction of particle-bubble collision efficiency in a turbulent flow was developed from a multiscale modelling perspective. A stationary bubble was positioned in the center of a "box" and particles moved from right to left in a turbulent flow. Increasing the intensity of turbulence was found to increase the efficiency of particle-bubble collision, which is consistent with the studies by Ngo-Cong et al. (2018). Discrete element method was used to study the collisions between a central bubble and falling particles in a quiescent flow (Gao et al., 2017; Maxwell et al., 2012). Fayed and Ragab (2013) studied the particle-bubble collision kernel using direct numerical simulation (DNS) in a homogeneous isotropic turbulence. The collision kernel is defined as the number of collisions per unit time per unit volume between two size groups per unit pair number density. It can be calculated as a function of the radial distribution function which is a measure of the effect of preferential concentration on the pair number density at contact. Preferential concentrations of particles and bubbles were observed in the turbulence and the segregated behavior of particles and bubbles led to reduced collision frequency between particles and bubbles.

Many efforts have been made to investigate the collisions between particles and bubbles and various models have been developed to describe the collision efficiency. Various simplifications and assumptions had to be made in the development of the theoretical particle-bubble collision models. In the modelling study of collisions between particles and bubbles, liquid flow around the bubbles has generally been simplified as Stokes flow or potential flow and particles are assumed to follow the streamlines of fluid around the bubble. In the development of the theoretical particle-bubble collision models, assumptions must be made regarding to liquid flows as turbulent flows are random and chaotic. There are limitations in applying experimental techniques to study particle-bubble collisions in turbulent flow environment, as experimental technique is not available in the study of particle-bubble collisions in the turbulent flows. 3D tracking of particle's movement in turbulent flows has always been a challenging subject. Visualizing turbulent flows simultaneously makes the problem nearly intractable. It is desirable to carry out rigorous numerical simulation of particle-bubble collisions in turbulent flow. In the current work, a DNS model for studying the effect of turbulence on the collisions between particles and bubbles will be reported. A statistical analysis of a group of particles and bubbles in the forced turbulent flow is performed to probe the mechanism of particle-bubble collision in a turbulent flow. The preferential distributions of particles and bubbles in the turbulence are different. this effect on the collisions between particles and bubbles attracts little attentions. This study will explore the effects of preferential distributions of particles and bubbles on the particle-bubble collisions.

2. Problem setup and numerical method

2.1. Problem description of a particle-bubble collision system

In order to keep the computations affordable, the simulation volume was restricted to a cubic domain. The collisions of bidisperse particles consisted of spherical particles and bubbles were simulated in a cubic domain defined as fully-periodic boundary conditions in all dimensions. This boundary condition means that, for example, the right boundary is connected to the left boundary logically and the fluids as well as the dispersed phases moving out of the right boundary will enter the domain immediately from the left boundary and so are the other two directions. It is assumed that the same particle-bubble collision behaviour in the simulated domain could be repeated within the whole flotation system. As shown in Fig. 2, a number of bidisperse spherical particles and bubbles are inserted into a reconstructed domain. Simulations of the collision process were performed in the reconstructed domain in a quiescent/turbulent environment, for different groups of particles and bubbles. We chose pyrite, one of the common minerals, with particle density ρ_p at 5000 kg/m^3 to represent minerals. The purpose of this study is to explore the effects of turbulence on the particle-bubble collisions. The role of turbulence acting on particles of different densities may be different, but we believe the effects will be in the same pattern. The sizes of particles and bubbles vary for different cases which will be illustrated in the following sections.

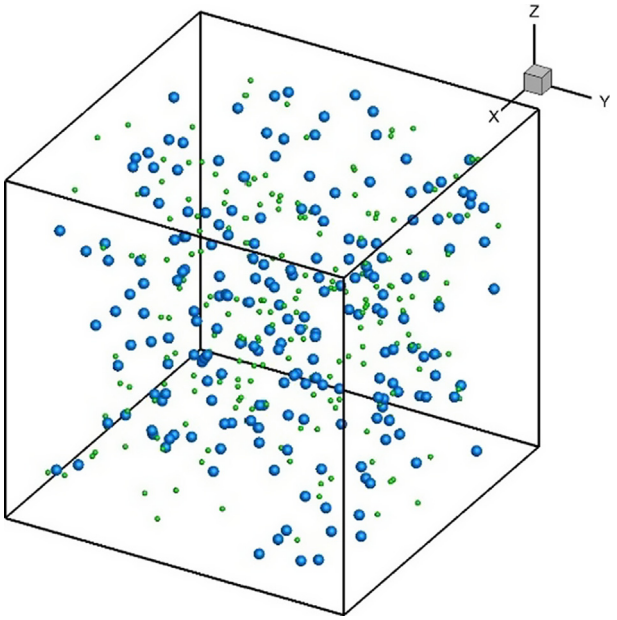

Fig. 2. Schematic diagram of a particle-bubble collision system with particles and bubbles randomly distributed in the cubic domain.

2.2. The pseudo-spectral method

The flow field contains a system of liquid (continuum phase) laden with solid particles and bubbles (disperse phases, hereinafter "particle" will be used generally if not specified particularly). The pseudo-spectral method is applied to solve the homogeneous isotropic turbulence and the computational domain is a cube with sides $L = 2\pi$ which is a requirement of the Fast Fourier Transforms. The code was originally developed by Ruetsch and Maxey (1991) and was used as a basis for studying the particle-settling problem and particle concentration field by Wang and Maxey (1993). For the present work, the incompressible Navier-Stokes equation along with the continuity equation:

$$\frac{\partial \vec{u}}{\partial t} = \vec{u} \times \vec{\omega} - \vec{\nabla}\left(\frac{p}{\rho} + \frac{\vec{u}^2}{2}\right) + \nu_f \vec{\nabla}^2(\vec{u}) + \vec{f} \tag{13}$$

$$\vec{\nabla} \cdot \vec{u} = 0 \tag{14}$$

were solved in spectral space. Here, $\vec{u}$ is the fluid velocity, $\vec{\omega} = \vec{\nabla} \times \vec{u}$

is the vorticity, p is the pressure, ν_f is the kinematic viscosity of the fluid and $\vec{f}$ is the forcing term which is used to generate and maintain the turbulence. The flow domain is uniformly discretized into N^3 with $N = 128$ in all the simulations and the time step size is $\Delta t = 1.0 \times 10^{-5}$ in spectral unit. For the time evolution, the second-order Adams-Bashforth scheme is applied for the nonlinear term, the second-order Crank-Nicholson scheme for the viscous term and the Euler scheme for the forcing term. More implementation details of the pseudo-spectral method and the algorithm can be found in the work by Wang and Rosa (2009).

Since the flow is generated from totally quiescent state and maintained by the forcing term, some basic information is given as follows. The wavenumber in spectral space is defined as $k_i = \pm n_i$ with $n_i = 0, 1, 2, \cdots, N/2$ and $i = 1, 2, 3$. For simplicity, a small portion of energy in the high wavenumbers $|\vec{k}| \geq (N-3)/2$ is neglected. The complex, vector-valued Uhlenbeck-Ornstein stochastic process is used in the Eswaran-Pope forcing scheme (Eswaran and Pope, 1988) to implement the artificial forcing term. The rate of total energy input is determined by three parameters: the forcing radius $k_F = \sqrt{8}$, the forcing amplitude σ_F which is varied to generate flow fields with different dissipation rates, and the forcing timescale $T_F = 0.038$. This setting is similar to that in Wang et al.'s work (2014) where additional relevant information can be referred.

2.3. Suspended particles

In the present work, the solid particles and bubbles have sizes that are comparable to the Kolmogorov length scale η_K of the turbulence. Therefore, they can be treated as point particles approximately and a simplified and modified form of the motion equation (Maxey and Riley, 1983) is applied to solve the motion of particles as:

$$\frac{dV_i}{dt} = \frac{(U_i + \widetilde{u}_i - V_i) f(Re_\alpha)}{\tau_\alpha} + \beta_\alpha \frac{DU_i}{Dt} + (1 - \beta_\alpha) g_i \tag{15}$$

where the subscript "i" denotes x, y and z directions, respectively, V_i is the particle velocity, U_i is the fluid velocity at the location of the particles and is determined numerically from the values of its neighboring grids using a six-point Lagrange interpolation scheme in each spatial direction, $\widetilde{u}_i$ is added to embed the hydrodynamic interactions (HDI) among particles and represents the disturbance flow velocities from surrounding particles, g_i is the gravity force, the subscript "α" denotes "p" for particle and "b" for bubbles, $\beta_\alpha = 3\rho_f/(\rho_f + 2\rho_\alpha)$ is a coefficient with ρ_f being the fluid density and ρ_α being the density of solid particles ρ_p or bubbles ρ_b, $\tau_\alpha = {r_\alpha}^2/3\nu_f\beta_\alpha$ is the response time of the particles τ_p or bubbles τ_b with r_α being the radius of solid particles r_p or bubbles r_b, $f(Re_\alpha)$ is the non-linear drag coefficient which is defined following Cerutti et al. (2000) as:

$$f(Re_\alpha) = \begin{cases} 1, & Re_\alpha < 1 \\ 1 + \frac{3.6}{{Re_\alpha}^{0.313}} \left(\frac{Re_\alpha - 1}{19}\right)^2, & 1 \leq Re_\alpha \leq 20 \\ 1 + 0.15 {Re_\alpha}^{0.687}, & Re_\alpha > 20 \end{cases} \tag{16}$$

where Re_α is particle Reynolds number defined as

$$Re_\alpha = \frac{2 r_\alpha |\vec{V} - \vec{U}|}{\nu_f} \tag{17}$$

In this simplified motion equation, the inertia term, fluid acceleration term, added mass term and Stokes drag term are considered, while the Basset history term and two high-order correction terms are neglected as most researchers have done (Squires and Eaton, 1991; Wang and Maxey, 1993; Wang et al., 2000), since the particles are small and the flow field is homogeneous. Typically, N_p particles and N_b bubbles, with diameters comparable to η_K, are introduced randomly into the flow field after statistically stationary state has been reached, or they are introduced directly in the simulation with a quiescent flow. And a fourth-order Adams-Bashforth method is used to advance the particles' motion.

It is important to notice that $\widetilde{u}_i$ is a key variable in the present simulation. To set $\widetilde{u}_i = 0$ means the HDI are neglected and it is totally a one-way simulation. In order to embed the HDI effect, an improved superposition method developed by Wang et al. (2005) is applied in the present simulation. In their method, the no-slip boundary condition is roughly satisfied on the surfaces of particles and bubbles with the assumption that the disturbance flows induced by the disperse phases can be modeled as quasi-steady Stokes flows. For the j^{th} particle at position $\boldsymbol{Y}_p^{(j)}$ with radius $r_p^{(j)}$ and velocity $\boldsymbol{V}^{(j)}$, the disturbance flow at position $\boldsymbol{x}$ is in the form of:

$$\begin{aligned} &\boldsymbol{u}_s[\boldsymbol{r}^{(j)}, \boldsymbol{V}^{(j)}] \\ &= \left[\frac{3}{4}\frac{r_p^{(j)}}{r^{(j)}} - \frac{3}{4}\left(\frac{r_p^{(j)}}{r^{(j)}}\right)^3\right] \frac{\boldsymbol{r}^{(j)}}{(r^{(j)})^2} \boldsymbol{V}^{(j)} \cdot \boldsymbol{r}^{(j)} + \left[\frac{3}{4}\frac{r_p^{(j)}}{r^{(j)}} + \frac{1}{4}\left(\frac{r_p^{(j)}}{r^{(j)}}\right)^3\right] \boldsymbol{V}^{(j)} \end{aligned} \tag{18}$$

where $\boldsymbol{r}^{(j)} = \boldsymbol{x} - \boldsymbol{Y}_p^{(j)}$. However, all the particles can affect each other theoretically. Therefore, the disturbance field $\widetilde{\boldsymbol{u}}^{(j)}(\boldsymbol{Y}_p^{(j)})$ at the location of the j^{th} particle due to the other particles has the following complex form:

$$\widetilde{\boldsymbol{u}}^{(j)}(\boldsymbol{Y}_p^{(j)}) = \sum_{m=1, m\neq j}^{N_p} \boldsymbol{u}_s[\boldsymbol{d}^{(mj)}, \boldsymbol{V}^{(m)} - \boldsymbol{U}^{(m)}(\boldsymbol{Y}_p^{(m)}) - \boldsymbol{u}^{(m)}] \tag{19}$$

where $\boldsymbol{d}^{(mj)} = \boldsymbol{Y}_p^{(j)} - \boldsymbol{Y}_p^{(m)}$. This is a coupled system which will consume lots of computational resources if all particles are interacting with each other. As Wang et al. (2005) pointed out, the Stokes flow induced by a particle decays with the increasing distance, which means that a truncation radius R_T could be applied to consider only the effect of neighboring particles. They also reported that collision efficiency as well as collision kernel are not sensitive to the truncation radius if $R_T \geq 20$ which is also used in the present simulation.

2.4. Collision statistics

To quantify the collision statistics in the system, the concept of collision kernel is used. The number of collision events in unit time and unit space, for the particle-particle collision or bubble-bubble collision, is:

$$\mathcal{N}_{\alpha\alpha} = \Gamma_{\alpha\alpha} \frac{n_\alpha^2}{2} \tag{20}$$

where the subscript "$\alpha\alpha$" denotes "pp" for particle-particle collisions and "bb" for bubble-bubble collisions (these are so-called self-collisions), respectively, $\Gamma_{\alpha\alpha}$ is the collsion kernel and $n_\alpha = N_\alpha/\Omega$ is the number density of N_p particles or N_b bubbles with Ω being the volume of the domain. For the particle-bubble collision, it is in the form of:

$$\mathcal{N}_{pb} = \Gamma_{pb} n_p n_b \tag{21}$$

The measurement of collision kernels can be done in two ways: one is dynamic and the other is kinematic. The dynamic kernels are based on the direct counting of collision events and their values at time t^n are:

$$\Gamma_{\alpha\alpha}^D(t^n) = \frac{2\Omega \times N_{\alpha c}(t^{n-1} \to t^n)}{\Delta t {N_\alpha}^2} \tag{22-a}$$

$$\Gamma_{pb}^D(t^n) = \frac{\Omega \times N_{pbc}(t^{n-1} \to t^n)}{\Delta t N_p N_b} \tag{22-b}$$

where $N_{\alpha c}(t^{n-1} \to t^n)$ is the number of collision events happening in the time interval $t^{n-1} \to t^n$ for particle-particle or bubble-bubble collisions and $N_{pbc}(t^{n-1} \to t^n)$ for particle-bubble collisions. Following the spherical formulation of kinematic kernel developed by Sundaram and Collins (2000) and Wang et al. (2000), the next formula is used in the present work:

$$\Gamma^{K}(t^n) = 2\pi R_c^2 \cdot \overline{|w_r|}(R_c) \cdot \overline{g}(R_c) \quad (23)$$

where R_c is the collision radius and equals $2r_p$, $2r_b$ or, $r_p + r_b$ for the collision of particle-particle, bubble-bubble or particle-bubble, respectively; $\overline{|w_r|}(R_c)$ is the radial relative velocity (RRV) and $\overline{g}(R_c)$ the radial distribution function (RDF) at contact, and "−" denotes the value averaged over all pairs. The RDF can be calculated as:

$$\overline{g}(R_c) = \frac{N_{pairs}(t^{n-1} \to t^n)/V_{shell}}{N_\alpha (N_\alpha - 1)/(2\Omega)} \quad (24\text{-a})$$

$$\overline{g}(R_c) = \frac{N_{pairs}(t^{n-1} \to t^n)/V_{shell}}{N_p N_b/\Omega} \quad (24\text{-b})$$

for self-collision of particles or bubbles and particle-bubble collision, respectively. Here, $N_{pairs}(t^{n-1} \to t^n)$ is the number of pairs that can be made in the shell $R_c - \delta < r < R_c + \delta$ with thickness $\delta = x\%R_c$ and volume V_{shell}, and specifically $x = 4$ is chosen. It identifies the prospective pairs participating in hydrodynamic interactions in the collision range. When the particles and bubbles are homogeneously distributed, the radial distribution function between prospective particle-bubble pairs is unity. Currently, we merely consider the effect of turbulence on the collisions among particles and unloaded bubbles. Therefore, a colliding pair would disappear at the collision location and will be relocated randomly in other locations with same properties. This simplifying assumption (motivated purely by computational limitations) has been made that bubbles and particles can be randomly relocated during the simulation, unlike what happens in reality, but the size of the effect that this simplifying assumption will have on our results is unknown.

3. Results and discussion

3.1. Effects of HDI on particle-bubble interactions

To further understand the effects of the hydrodynamic interactions among particles and bubbles, dynamics of particles and bubbles in a homogeneous isotropic turbulence are reported. We consider a system containing 10 000 particles and 10 000 bubbles in a 128^3 DNS simulation. The continuum phase is water with density of 1000 g/cm^3 and kinematic viscosity of 0.01 cm^2/s. The parameters of the particle-bubble collision system and the background flow are shown in Table 1. The terminal velocity is −1.78 cm/s for particles and 3.46 cm/s for bubbles when interactions among particles and bubbles are not considered.

The probability distributions of particle's velocity and bubble's velocity in three directions are plotted respectively in Figs. 3 and 4. All velocities followed closely the Gaussian distribution in the homogeneous isotropic turbulence. When hydrodynamic interactions were considered, the mean velocity of the particles in the gravitational direction changed from −1.78 cm/s to +0.55 cm/s, whilst the distributions in the other two directions remained unchanged. It is considered that particles in the vicinity of rising bubbles were carried in the upward direction, resulting in the increased mean velocity of particles in the gravitational direction, from downward to upward. Similar trends can also be observed for bubbles. When hydrodynamic interactions are considered, the distribution of bubbles' velocity in the gravitational direction shifted to the right where the mean value changed from +3.46 cm/s to +5.73 cm/s, whilst the distributions in the other two directions remained unchanged. The trajectories of particles and bubbles with and without hydrodynamic interactions are shown in Fig. 5. It was observed that the movement of particles was more chaotic when considering the perturbations from bubbles.

3.2. Particle-bubble collision efficiency in quiescent liquid

The particle-bubble collision efficiency can be affected by many factors, such as particle size and volume fraction, particle density, bubble size and volume fraction, bubble rising velocity and turbulence intensity. The effects of particle size and bubble size on particle-bubble collision efficiency in a quiescent liquid are studied in this section. The information of the particle-bubble collision system in a quiescent liquid is provided in Table 2.

Particle-bubble collision efficiency is calculated as a ratio of real collision events to ideal collision events. In this case where liquid is quiescent, collision efficiency can be represented by the ratio of collision kernel considering HDI effects to collision kernel without HDI effects. Due to the differences in the assumptions which had been made in the development of the particle-bubble collision models, the predictions for the collision efficiency from these models can be very different from one another. Fig. 6 shows collision efficiency as a function of bubble diameter. Collision efficiency between particles and bubbles decreased with increasing bubble diameter. This is in accordance to the previous findings that smaller bubbles could increase the probability of collision (Ahmed and Jameson, 1985; Hassanzadeh et al., 2016; Tao, 2005; Yoon and Luttrell, 1989). This does not mean that flotation process should use bubbles as small as possible. Small bubbles would come out of the flotation process in the tailings causing loss of valuable minerals. It should be noted that the low carrying capacity of small bubbles is another limitation. Therefore, small bubbles in combination with larger ones could be used to obtain the best recoveries (Ahmed and Jameson, 1985). Another factor to consider is the particle size and there is an optimum bubble size which is depended on the particle size (Lakghomi et al., 2015). A successful flotation process should consider collision, attachment and detachment as integral. Nevertheless, these three subprocesses should be separately studied to improve the fundamental understandings of interactions between particles and bubbles. The effect of bubble size on the flotation process (collision, attachment and detachment) has been widely studied (Ahmed and Jameson, 1985; Tao, 2005; Yoon and Luttrell, 1989). This study intends to isolate collision from attachment and detachment, and study solely the effects of turbulence on collision process.

Fig. 7 shows the effect of particle diameter on the collision efficiency between particles and bubbles. The effect of particle size on flotation performance has been widely studied. In the early stage, Gaudin et al. (1931) found that particle collection efficiency is closely dependent on particle size. Initially, flotation recovery increases with particle size monotonically and reaches a plateau. Afterwards, flotation recovery plummets with increase in particle size (Gontijo et al., 2007; Dobby and Finch, 1987; Gaudin et al., 1931; Wang et al., 2016). Particle-bubble collision is the limiting factor for fine particles recovery due to their small inertia and low collision efficiency. Fine particles follow the streamlines as they do not have large enough inertia to remarkably deviate from the fluid streamlines at their close approach to the bubble surface. Therefore, fine particles can be easily swept past the bubble surface without contacting, resulting in low collision efficiency. On the contrary, collision is not a problem for coarse particles

Table 1
Parameters of the HDI simulation of a turbulent flow.

Parameters	Values
Domain size	9.28 cm × 9.28 cm × 9.28 cm
Grid size	725 μm
Grid number	128^3
Particle diameter	60 μm
Particle volume fraction	1.410^{-6}
Bubble diameter	300 × μm
Bubble volume fraction	1.8×10^{-4}
Energy dissipation rate	1.0 cm^2/s^3
Kolmogorov length scale	330 μm
Kolmogorov time scale	0.1 s
Eddy turnover time	2.1 s
Simulation time	26.8 s
Statistic time interval	8.4 s

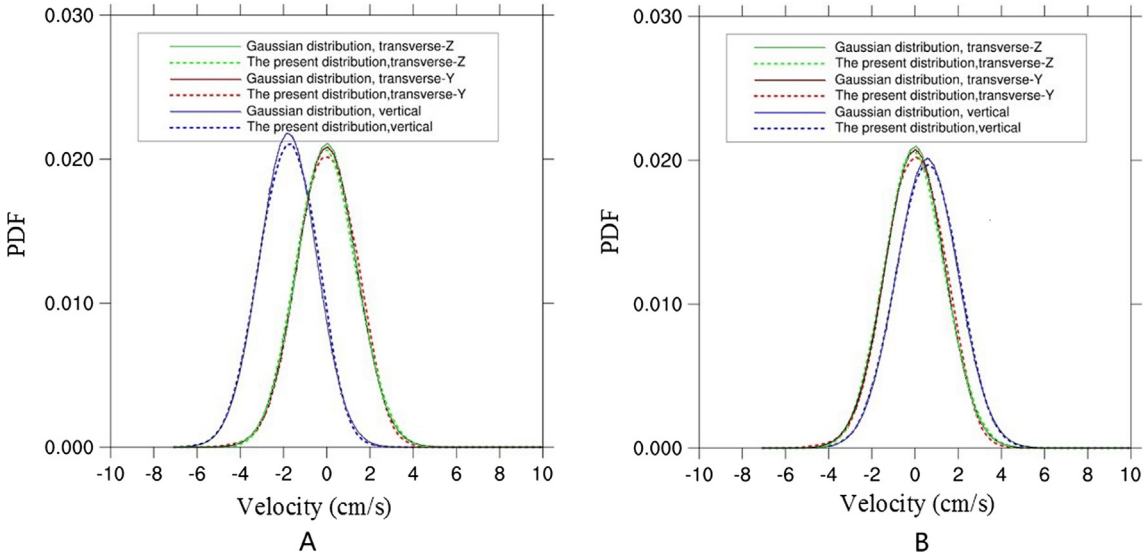

Fig. 3. The probability distribution function of particles' velocities (A: without HDI effect; B: with HDI effect).

(Jameson, 2010a). Coarse particles, after forming particle-bubble aggregates, are vulnerable to disturbances from turbulent liquid motion resulting in particle detachment.

Though collision efficiency models and our DNS results all indicate that collision efficiency increased with increasing particle size, an optimum particle size is present for overall efficient recovery. It was noted that the collision process was affected by the diameters of particle and bubble. Collision probabilities in quiescent flotation conditions were compared to the collision efficiency models and the model provided by Flint and Howarth gave the closest agreement with the DNS data. Both our DNS results and collision efficiency models indicate that decreasing bubble size and increasing particle size can increase particle-bubble collision efficiency. Flotation is a complicated process and is affected by many parameters. Studying the effects of single factors, in our case particle size and bubble size, on flotation recovery is helpful to understand the mechanisms of interactions between particles and bubbles. For treatment of a particular mineral, combined effects of these parameters should be considered.

3.3. Particle-bubble collision in a forced homogeneous isotropic turbulence

Turbulence is another important parameter that affects collisions between particles and bubbles. When simulating the effect of turbulence on particle-bubble collisions, the parameters of the collision system and the background flow are given respectively in Tables 3 and 4. The sizes of particle and bubble are chosen to give the same relaxation time, therefore identical Stokes numbers ($St_\alpha = \tau_\alpha/\tau_K$) for particles and bubbles are used as indicated in Fig. 8.

We want to investigate the effect of turbulence intensity (turbulent dissipation rate) on collisions between particles and bubbles. For single phase turbulent flow based on spectral simulation, a sufficient grid resolution is required to resolve the Kolmogorov length vortices. It is noted that the physical domain size is quite small to ensure our grid resolution. Periodic boundary conditions are applied in all three directions and results are considered representative in turbulent flow fields.

Present tendencies of process intensification in industry employ hydrodynamical techniques of high turbulent intensities to enhance collisions between particles and bubbles. Static mixer and hydrodynamic cavitation has been applied to generate fine bubbles (Yoon

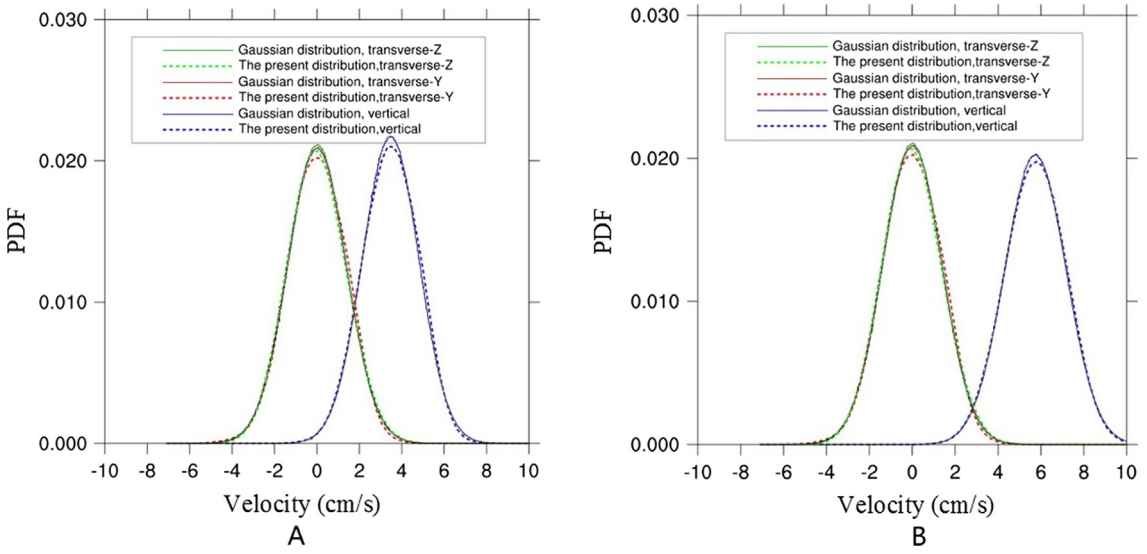

Fig. 4. The probability distribution function of bubbles' velocities (A: without HDI effect; B: with HDI effect).

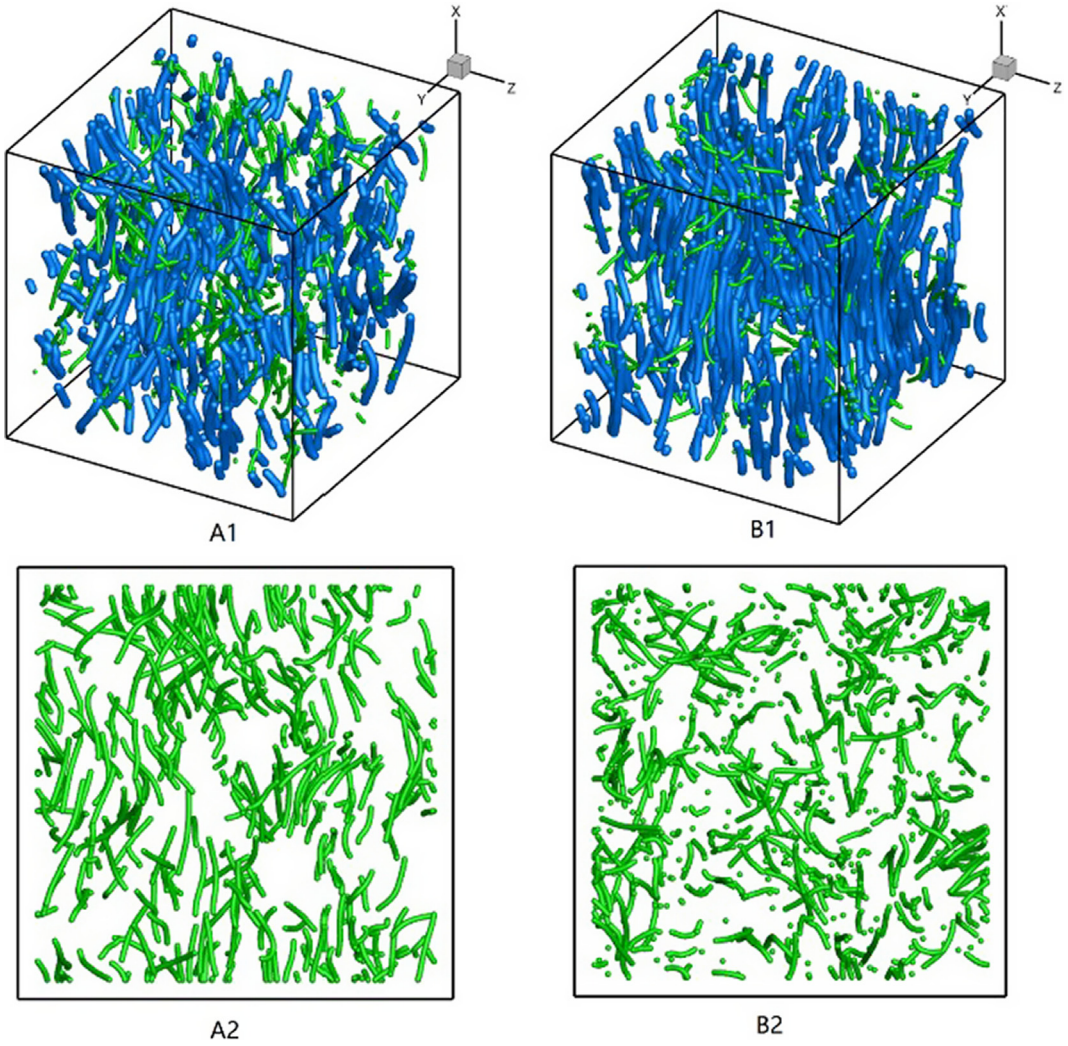

Fig. 5. The trajectories of particles (green) and bubbles (blue) in a short period (A1: without HDI; B1: with HDI; A2: projection of A1 in x-z plane; B2: projection of B1 in x-z plane). (For interpretation of the references to colour in this figure legend, the reader is referred to the web version of this article.)

Table 2
Parameters of the particle-bubble collision system in a quiescent liquid.

Parameters	Values
Domain size	9.60 cm × 9.60 cm × 9.60 cm
Grid size	750 μm
Grid number	128^3
Particle volume fraction	0.001%
Bubble volume fraction	0.100%
Time step	0.2 ms
Number of time steps	50,000 (The first 20,000 time steps are discarded when conducting statistics)

et al., 1984; Zhang et al., 2013). A plunging jet has been used to generate fine bubbles and create a high shear region where the efficiency of collision between particles and bubbles can be substantially enhanced (Jameson, 1988, 2010b). High turbulent flow fields are present in these situations. In the turbulent flow field, particles accumulate in specific regions, being called "preferential concentration". Particles, with density higher than the liquid, tend to migrate from the eddy core and concentrate on the edges of the eddy (Crowe et al., 1995). Bubbles exhibit different characteristics compared to the behavior of particles and bubbles are pushed towards the eddy axis (Chahine, 1995). It is believed that their different tendencies in "preferential concentrations"

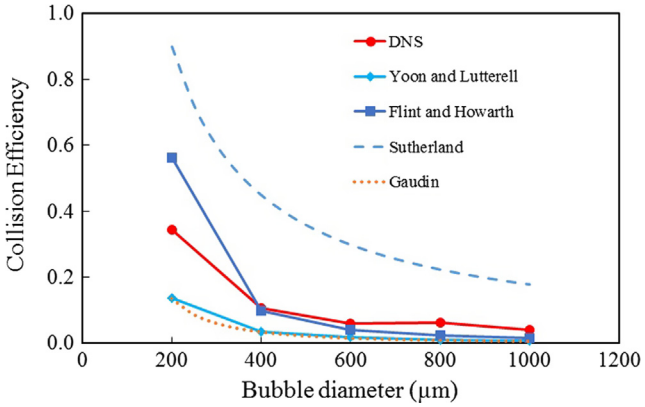

Fig. 6. The effect of bubble diameter on the collision efficiency between particles and bubbles (The diameter of particles is 60 μm).

would cause local separation of particles and bubbles, and therefore affect the collision frequency between particles and bubbles. A snapshot of the distributions of particles and bubbles in the turbulent field is shown in Fig. 9. The distributions of particles and bubbles would be different for different turbulence intensities.

To investigate the effects of turbulence on particle-bubble collisions, turbulent dissipation rates varied from 0.1 to 10.8 m^2/s^3 as in Fig. 8.

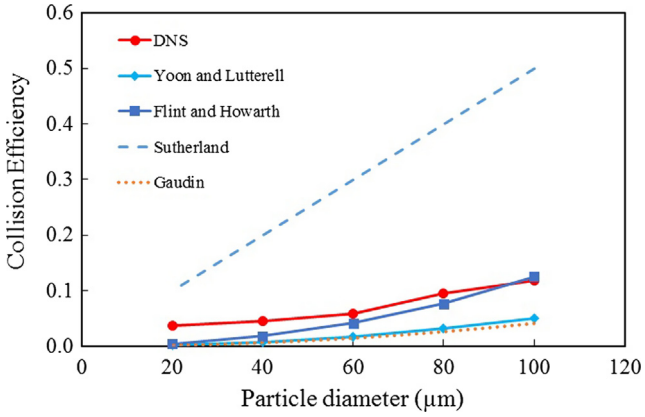

Fig. 7. The effect of particle diameter on the collision efficiency between particles and bubbles (The diameter of bubbles is 600 μm).

Table 3
Parameters of the particle-bubble collision system in turbulent flow.

Parameters	Values
Domain size	0.50 cm × 0.50 cm × 0.50 cm
Grid size	39 μm
Grid number	128^3
Particle diameter	57 μm
Particle volume fraction	10%
Bubble diameter	190 μm
Bubble volume fraction	10%
Time step	0.006 ms
Number of time steps	50,000 (The first 20,000 time steps are discarded when conducting statistics)

Table 4
Parameters of the background flow.

Statistics	Case1	Case2	Case3	Case4	Case5
Turbulent dissipation rate (m^2/s^3)	0.1	0.7	1.1	3.0	10.8
Kolmogorov length scale (μm)	54	34	31	24	17
Kolmogorov time scale (ms)	3.0	1.2	1.0	0.6	0.3
Fluctuation velocity (cm/s)	5.0	9.8	11.4	16.0	25.4
Taylor microscale Reynolds number	30	44	49	57	77
Integral length scale (μm)	1057	939	917	866	871

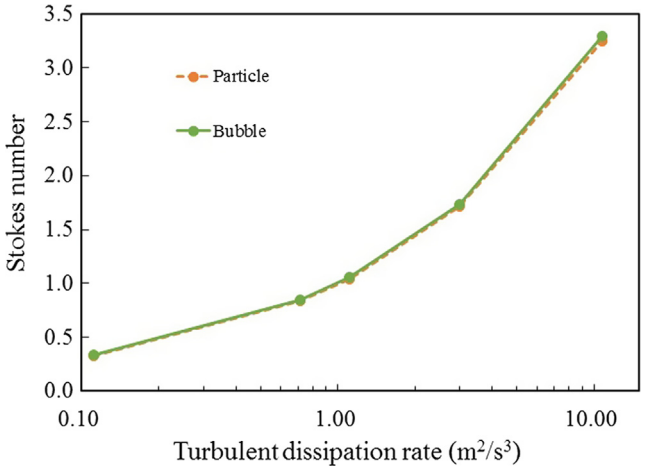

Fig. 8. Particle and bubble Stokes numbers in flow fields with different turbulent dissipation rates.

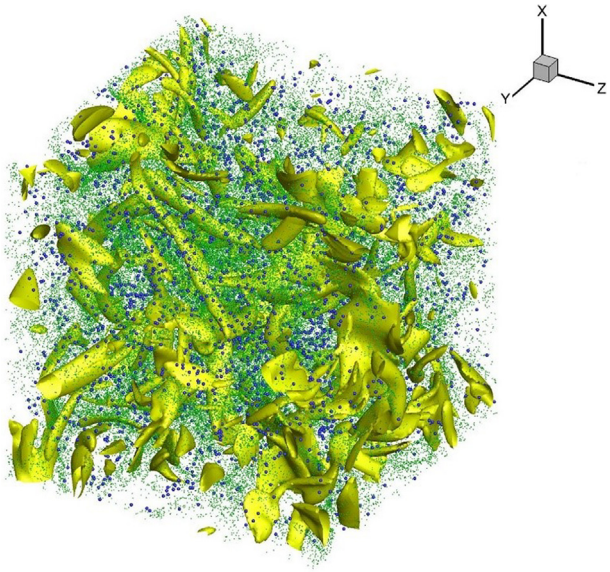

Fig. 9. Particles (green dots) and bubbles (blue dots) in a 3D vorticity field (the iso-surface of vorticity has a value of 2000 1/s). (For interpretation of the references to colour in this figure legend, the reader is referred to the web version of this article.)

Three cases were selected to present the effect of turbulence on the distributions of particles and bubbles as is shown in Fig. 10. Preferential concentration is dependent on the interplays of particles and bubbles, and it is most apparent when Stokes number is near 1 (Wang and Maxey, 1993). In our settings, relaxation times of particles and bubbles are identical meaning that Stokes number of particles and bubbles under different turbulent conditions would be identical. Particles and bubbles were initially evenly distributed. Fig. 10 B shows distinct local enrichment of particles and bubbles in the turbulent flow as Stokes number is slightly above 1. This is more apparent in Fig. 11 where the distributions of particles and bubbles are separately plotted with vorticity contours in the background. Heavy particles are shown to accumulate in the edges of the vortex structures and bubbles are shown to accumulate in the center of the vortices. It is hypothesized that the contrasting effect of preferential concentrations of particles and bubbles lead to diminished collisions between particles and bubbles.

Two different methods, a dynamic approach and a kinematic approach as described in Section 3.2, are used to study the effects of turbulent dissipation rate on the collisions among particles and bubbles. Fig. 12 shows that kinematic kernels of particle-particle, bubble-bubble and particle-bubble match well with dynamic ones. Collision kernels of pairs of particle-particle, bubble-bubble and particle-bubble are studied separately. All collisions increased with increasing turbulent dissipation rate. It is straightforward to understand that increasing turbulence would enhance collisions of particle-particle and bubble-bubble as preferential concentration resulting in accumulation effects leads to higher likelihood of collisions between particles of the same type. Collisions between particles and bubbles should be analyzed to study the effect of turbulence. Turbulence affects particle-bubble collisions by two mechanisms, namely, turbulent fluctuations that cause relative motion between particles and bubbles and the preferential concentration that leads to a highly intermittent local pair density distribution (Wang et al., 2000). Following the description of kinematic collision kernel, these two effects of turbulence can be represented individually by radial relative velocity and radial distribution function.

Fig. 13 shows the radial relative velocity of particle-particle, bubble-bubble and particle-bubble as a function of turbulent dissipation rate. The relative velocity between two colliding particles is considered to be dominated by large-scale energetic eddies. The contribution of the relative velocity to the collision kernel is termed the turbulent transport

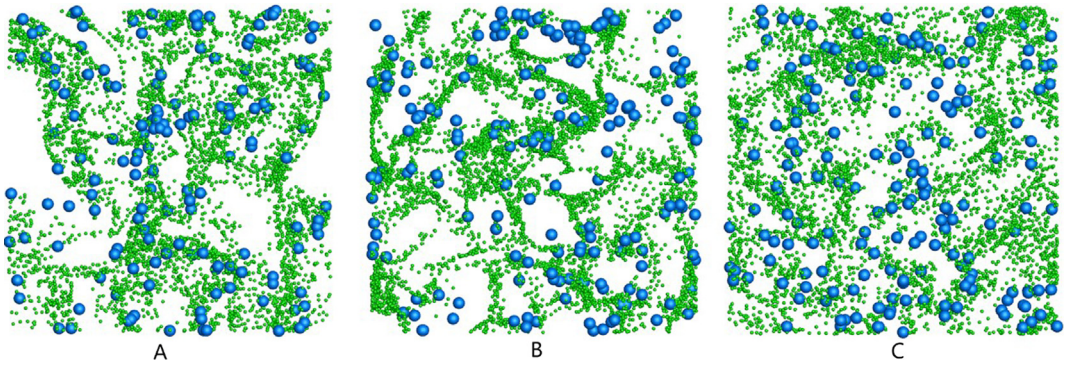

Fig. 10. The distribution of particles and bubbles in flow fields with different dissipation rates and Stokes numbers (A: 0.1 m^2/s^3, St = 0.3; B: 1.1 m^2/s^3, St = 1.1; C: 10.8 m^2/s^3, St = 3.3).

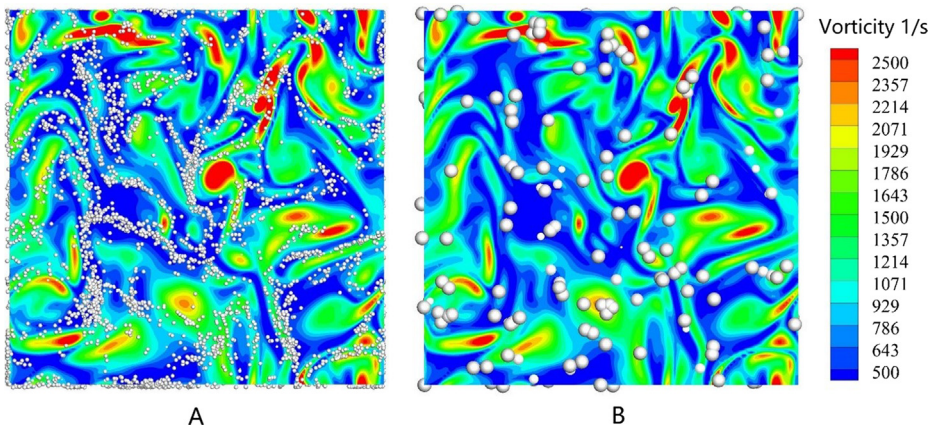

Fig. 11. The different distribution pattern of particles (A) and bubbles (B) in a y-z slice of vorticity (turbulent dissipation rate at 1.1 m^2/s^3).

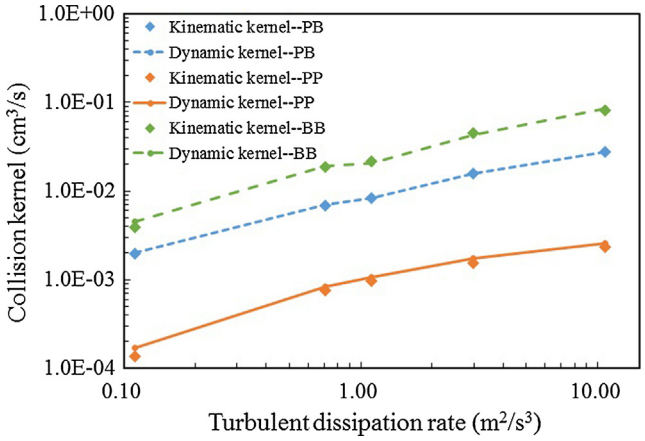

Fig. 12. The increase of collision kernel with the increase of turbulent dissipation rate.

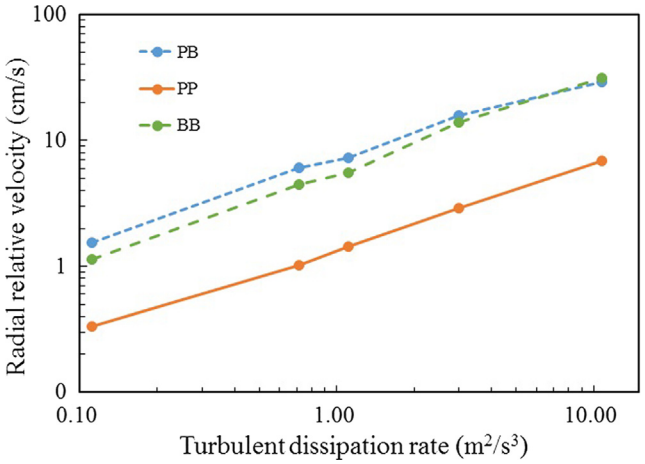

Fig. 13. The dependence of radial relative velocity with turbulent dissipation rate.

effect (Wang et al., 2000). All radial relative velocities increase quickly with turbulent dissipation rate because large-scale turbulent fluctuations contribute to the chaotic motion of particles and bubbles. The radial relative velocities of collision pairs (particle-particle, bubble-bubble and particle-bubble) follow the same trend as collision kernels. In the flotation process, relaxation times of particles and bubbles are much smaller than the large eddy turnover time. In this range, radial relative velocities of collision pairs increase quickly with turbulent dissipation rate. To evaluate whether particle-bubble collisions decrease with turbulence intensity in a particular range, it is necessary to quantify the effect of preferential concentrations of particles and bubbles.

Preferential concentration of particles and bubbles can be characterized by the particle radial distribution function. The radial distribution functions of pairs of particle-particle, bubble-bubble and particle-bubble are calculated and presented in Fig. 14. The values are obtained by averaging over many time samples and they are limiting values of the radial distribution function at contact. When there is no preferential concentration, the RDF at contact is always one theoretically. Apparent peaks are formed for pairs of particle-particle and bubble-bubble, meaning the accumulation effect of particles and bubbles are most apparent when turbulent dissipation rate is around 1 m^2/s^3 where the Stokes number of particles and bubbles is around 1. The

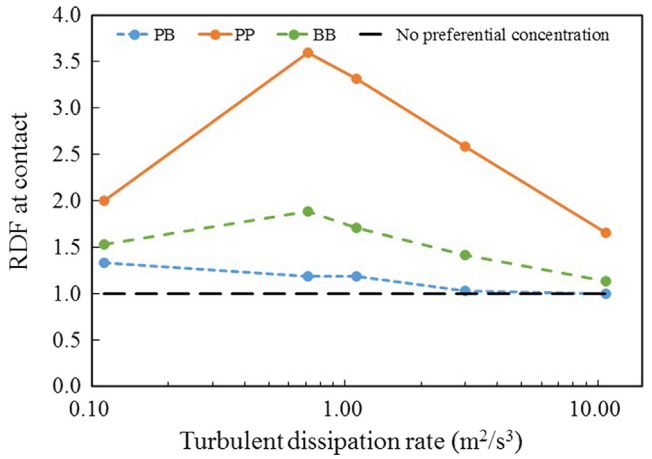

Fig. 14. The changes of radial distribution function with turbulent dissipation rate.

accumulating effect of particles (or bubbles) increases their chance for self-collisions. It is interesting to note that the radial distribution function for particle-bubble pairs does not change much with turbulent dissipation rate. It was assumed that a dimple would be present in the curve of radial distribution function between particles and bubbles when their Stokes number is around 1 because particles tend to accumulate on the edges of the eddy and bubbles tend to accumulate towards the eddy axis. This contrasting trend results in local separation of particles from bubbles. In the homogeneous isotropic turbulence, bubbles would find particles evenly distributed in the edges of eddy. The movements of particles and bubbles are forced to change with turbulent structures. Moreover, the effects of turbulence on the movement of particles and bubbles are dynamic as the turbulent structures are evolving and chaotic.

The system we studied was relatively simple in a way that particles and bubbles collide in a homogeneous isotropic turbulence and the flow domain was periodic in all directions. A sensitivity test on the effect of the size of the domain was made where the domain size was doubled and therefore the number of particles and bubbles are increased by eight times to maintain the volume fraction constant. Collision kernel, radial relative velocity and radial distribution function are very close for two simulation cases with different domain sizes. It should be mentioned that the original domain size was five times of the integral length scale, which is considered to be sufficient to include large scales in turbulent flows. The effects of turbulence on the collisions between particles and bubbles were studied from two perspectives: the effects of turbulent transport and the local accumulation effect. Particles and bubbles were observed to accumulate differently according to turbulent dissipation rate. Most apparent local accumulation effect was found when Stokes number was close to 1. The radial distribution function of particle-bubble pair was not changed much in turbulent fields of different intensities. The decrease of radial distribution function between particles and bubbles is about 30% with the increase of turbulence intensity in our simulations. Comparing the contribution of radial relative velocity and radial distribution function to the collision kernel, the contribution of radial distribution function could be neglected because the radial relative velocity increases by about 1900% (from 1.55 cm/s to 28.87 cm/s) while the radial distribution function decreases by only 33% (from 1.33 to 1.00). As radial relative velocities between particles and bubbles increased with turbulent dissipation rate, particle-bubble collision kernel was found to increase with turbulent dissipation rate. Nevertheless, this does not mean that we should intuitively increase turbulence intensity to enhance flotation process. Not to mention vortices would destabilize the attached particles on the surface of bubbles, but also the interaction time between particles and bubbles is reduced in highly turbulent field which adversely affects the attachment of particles to bubbles. The effect of turbulence on the attachment of particles to bubbles remains an open question, as it is still unclear how turbulence affects contact time and induction period. To efficiently enhance flotation process by modulating turbulence intensity, collision, attachment and detachment should be combined as a whole process where turbulence plays a crucial role.

3.4. Discussions

Flotation is a complex process involving surface chemistry, multiphase flows and turbulence. We have made a few simplifications in the simulations. In a real situation, the particle may or may not attach to the surface of a bubble after collision. If the particle is attached to the surface of a bubble, the bubble with attached particles would behave differently, which is a complex problem by itself. Currently, we merely consider the effect of turbulence on the collisions between particles and bubbles. Therefore, a colliding pair would disappear at the collision location and would be relocated randomly in other locations with same properties. The simplifying assumption (motivated purely by computational limitations) has been made that bubbles and particles can be randomly relocated during the simulation, unlike what happens in reality, but the size of the effect that this simplifying assumption will have on our results is unknown. We understand this treatment is artificial and cannot reflect the real situation, where collision, attachment and detachment can occur in the flotation process. Nevertheless, the study of collision isolated from attachment and detachment processes can achieve more fundamental understandings on the colliding interactions between particles and bubbles in flotation process. In addition, we have assumed the no-slip boundary condition in our treatments of particles and bubbles. In the modeling of flotation kinetics, the mobility of the bubble surface has always been problematic. It is either assumed to be mobile or immobile so the liquid flow around the bubble can be simplified as potential flow or Stokes flow. The real situation can be much more complex as the surface is partially mobile due to partial attachment of surfactants.

From the definition of the kinematic collision kernel, changes in radial distribution function would cause changes in the collision kernel. The particles and bubbles are not well-separated, which may result in the radial distribution function between particles and bubbles larger than 1.0. Nevertheless, we observe gradual increase in collision kernel. But this does not mean the effect of preferential concentration on the collision kernel can be neglected. In a way, it means that the effect of radial distribution function is overwhelmed by the effect of radial relative velocities. This is due to the fact that the sizes of bubbles are larger than the Kolmogorov length scales of the flotation system. Due to the intensification of flotation process, bubble mineralization is generally carried out in high turbulent flows, where bubbles are generally larger than the smallest scales (the Kolmogorov length scale). Nevertheless, the point-particle model is generally applied to systems where the size of dispersed phases is smaller than the Kolmogorov length scale of the turbulent field.

In our flotation simulation, the sizes of particles and bubbles are just comparable to (not much smaller than) the Kolmogorov length scale of turbulence. It seems that our application of point particle method to flotation is not completely appropriate, but considering the turbulence intensity of the flotation environment particles and bubbles are generally larger than the Kolmogorov scale. Only in calm flotation process such as flotation column, particles and bubbles are larger than the Kolmogorov scale. The hybrid superposition method has been proved to be an effective way to include the disturbance of dispersed phase in point particle method. Understandably, it is more accurate to use particle-resolved method to simulate the phenomena, which is computationally unaffordable at this stage. Therefore, we choose to relax the constraints for its application to the flotation.

4. Conclusions

A pseudo-spectral DNS model was successfully applied to gain a better insight into the collision behaviour of a bidisperse system consisting of spherical particles and bubbles. The simulations of particle-bubble collisions were conducted in both quiescent and homogeneous isotropic turbulent flows for the purpose of testing existing models of particle-bubble collisions, and to study the effects of varying levels of turbulence on the collisions between particles and bubbles. It was found that the collision process was affected by the diameters of particle and bubble. Out of the collision efficiency models considering the gravitational effect, the model provided by Flint and Howarth yield the closest agreement with the DNS data. DNS results and collision efficiency models all indicated that decreasing bubble size and increasing particle size could increase particle-bubble collision efficiency. The radial relative velocities between particles and bubbles increased with turbulent dissipation rate. The effects of preferential concentrations of particles and bubbles on the particle-bubble collision kernel were overwhelmed by the effects of radial relative velocities over the examined range of flow conditions. Collisions between particles and bubbles increased with turbulent dissipation rate as the relative movements of particles and bubbles are more chaotic in turbulent fields. It should be mentioned that a simplifying assumption (motivated purely by computational limitations) has been made that bubbles and particles can be randomly relocated during the simulation, unlike what happens in reality, but the size of the effect that this simplifying assumption will have on our results is unknown.

Author contribution statement

Dongdong Wan compiled the code and designed methodology.

Xuan Yi, Lian-Ping Wang, Xun Sun and Songying Chen did post-processing and helpful discussions.

Guichao Wang was responsible for the formulation and evolution of the research topic and for ensuring that the descriptions are accurate and agreed by all authors.

Declaration of Competing Interest

The authors declare that they have no competing financial interests or personal relationships that could have appeared to influence the work reported in this paper.

Acknowledgements

We gratefully acknowledge that this work was supported by Young Scholars Program of Shandong University, “YSPSDU 31360088964058” and National Natural Science Foundation of China through grants 91852205, 91852205 and 91741101, and by the U.S. National Science Foundation (NSF) under grants CNS1513031 and CBET-1706130. Computing resources are provided by the Center of Computational Science and Engineering at the Southern University of Science and Technology, and by National Center for Atmospheric Research through CISL-UDEL0001.

References

Ahmed, N., Jameson, G.J., 1985. The effect of bubble size on the rate of flotation of fine particles. Int. J. Miner. Process. 14, 195–215.
Ahmed, N., Jameson, G.J., 1989. Flotation kinetics. Miner. Process. Extr. Metall. Rev. 5, 77–99.
Brabcová, Z., Karapantsios, T., Kostoglou, M., Basařová, P., Matis, K., 2015. Bubble–particle collision interaction in flotation systems. Colloids Surf., A 473, 95–103.
Cerutti, S., Knio, O.M., Katz, J., 2000. Numerical study of cavitation inception in the near field of an axisymmetric jet at high Reynolds number. Phys. Fluids 12, 2444–2460.
Chahine, G., 1995. Bubble interactions with vortices. In: Green, S. (Ed.), Fluid Vortices. Springer, Netherlands, pp. 783–828.
Crowe, C.T., Troutt, T.R., Chung, J.N., 1995. Particle interactions with vortices. In: Green, S. (Ed.), Fluid Vortices. Springer, Netherlands, pp. 829–861.
Dai, Z., Dukhin, S., Fornasiero, D., Ralston, J., 1998. The inertial hydrodynamic interaction of particles and rising bubbles with mobile surfaces. J. Colloid Interface Sci. 197, 275–292.
Dai, Z., Fornasiero, D., Ralston, J., 2000. Particle–bubble collision models — a review. Adv. Colloid Interface Sci. 85, 231–256.
De F Gontijo, C., Fornasiero, D., Ralston, J., 2007. The limits of fine and coarse particle flotation. The Can. J. Chem. Eng. 85, 739–747.
Deglon, D.A., Sawyerr, F., O'Connor, C.T., 1999. A model to relate the flotation rate constant and the bubble surface area flux in mechanical flotation cells. Miner. Eng. 12, 599–608.
Dobby, G.S., Finch, J.A., 1987. Particle size dependence in flotation derived from a fundamental model of the capture process. Int. J. Miner. Process. 21, 241–260.
Eswaran, V., Pope, S.B., 1988. An examination of forcing in direct numerical simulations of turbulence. Comput. Fluids 16, 257–278.
Fayed, H.E., Ragab, S.A., 2013. Direct numerical simulation of particles-bubbles collisions kernel in homogeneous isotropic turbulence. J. Comput. Multiphase Flows 5, 167–188.
Flint, L., Howarth, W., 1971. The collision efficiency of small particles with spherical air bubbles. Chem. Eng. Sci. 26, 1155–1168.
Gao, Y., Evans, G.M., Wanless, E.J., Moreno-Atanasio, R., 2017. DEM modelling of particle-bubble capture through extended DLVO theory. Colloids Surf., A 529, 876–885.
Gaudin, A.M., 1957. Flotation. McGraw-Hill.
Gaudin, A.M., Groh, J.O., Henderson, H.B., 1931. Effect of particle size in flotation. Am. Inst. Mining Eng. Tech. Publ. 3–23.
Hassanzadeh, A., Firouzi, M., Albijanic, B., Celik, M.S., 2018. A review on determination of particle–bubble encounter using analytical, experimental and numerical methods. Miner. Eng. 122, 296–311.
Hassanzadeh, A., Hassas, B.V., Kouachi, S., Brabcova, Z., Çelik, M.S., 2016. Effect of bubble size and velocity on collision efficiency in chalcopyrite flotation. Colloids Surf., A 498, 258–267.
Heiskanen, K., 2000. On the relationship between flotation rate and bubble surface area flux. Miner. Eng. 13, 141–149.
Jameson, G., Nam, S., Young, M.M., 1977. Physical factors affecting recovery rates in flotation. Miner. Sci. Eng. 9, 103–118.
Jameson, G.J., 1988. A new concept in flotation column design. Column Flotation 88, 281–286.
Jameson, G.J., 2010a. Advances in fine and coarse particle flotation. Can. Metall. Q. 49, 328–330.
Jameson, G.J., 2010b. New directions in flotation machine design. Miner. Eng. 23, 835–841.
Klassen, V.I., Mokrousov, V.A., 1963. An introduction to the theory of flotation. Butterworths.
Lakghomi, B., Lawryshyn, Y., Hofmann, R., 2015. A model of particle removal in a dissolved air flotation tank: Importance of stratified flow and bubble size. Water Res. 68, 262–272.
Liu, T.Y., Schwarz, M.P., 2009a. CFD-based modelling of bubble-particle collision efficiency with mobile bubble surface in a turbulent environment. Int. J. Miner. Process. 90, 45–55.
Liu, T.Y., Schwarz, M.P., 2009b. CFD-based multiscale modelling of bubble–particle collision efficiency in a turbulent flotation cell. Chem. Eng. Sci. 64, 5287–5301.
Maxey, M.R., Riley, J.J., 1983. Equation of motion for a small rigid sphere in a nonuniform flow. Phys. Fluids 26, 883–889.
Maxwell, R., Ata, S., Wanless, E., Moreno-Atanasio, R., 2012. Computer simulations of particle–bubble interactions and particle sliding using discrete element method. J. Colloid Interface Sci. 381, 1–10.
Meyer, C.J., Deglon, D.A., 2011. Particle collision modeling - A review. Miner. Eng. 24, 719–730.
Morris, T., 1952. Measurement and evaluation of the rate of flotation as a function of particle size. Min. Eng. 4, 794–798.
Ngo-Cong, D., Nguyen, A.V., Tran-Cong, T., 2018. Isotropic turbulence surpasses gravity in affecting bubble-particle collision interaction in flotation. Miner. Eng. 122, 165–175.
Nguyen, A.V., An-Vo, D.-A., Tran-Cong, T., Evans, G.M., 2016. A review of stochastic description of the turbulence effect on bubble-particle interactions in flotation. Int. J. Miner. Process. 156, 75–86.
Nguyen Van, A., Kmeť, S., 1992. Collision efficiency for fine mineral particles with single bubble in a countercurrent flow regime. Int. J. Miner. Process. 35, 205–223.
Nutt, C., Kemp, M., Weston, J., 1963. Rate of flotation in a hallimond tube. Nature 197, 40–42.
Ruetsch, G., Maxey, M., 1991. Small-scale features of vorticity and passive scalar fields in homogeneous isotropic turbulence. Phys. Fluids A 3, 1587–1597.
Schulze, H., 1989. Hydrodynamics of bubble-mineral particle collisions. Miner. Process. Extractive Metall. Rev. 5, 43–76.
Schulze, H.J., Radoev, B., Geidel, T., Stechemesser, H., Töpfer, E., 1989. Investigations of the collision process between particles and gas bubbles in flotation - A theoretical analysis. Int. J. Miner. Process. 27, 263–278.
Squires, K.D., Eaton, J.K., 1991. Preferential concentration of particles by turbulence. Phys. Fluids A 3, 1169–1178.
Sundaram, S., Collins, L.R., 2000. Collision statistics in an isotropic particle-laden turbulent suspension. Part 1. Direct numerical simulations. J. Fluid Mech. 335, 75–109.
Sutherland, K., 1948. Physical chemistry of flotation. XI. Kinetics of the flotation process. J. Phys. Chem. 52, 394–425.
Tao, D., 2005. Role of bubble size in flotation of coarse and fine particles—a review. Sep. Sci. Technol. 39, 741–760.

Verrelli, D.I., Bruckard, W.J., Koh, P.T.L., Schwarz, M.P., Follink, B., 2014. Particle shape effects in flotation. Part 1: Microscale experimental observations. Miner. Eng. 58, 80–89.
Verrelli, D.I., Koh, P.T.L., Nguyen, A.V., 2011. Particle–bubble interaction and attachment in flotation. Chem. Eng. Sci. 66, 5910–5921.
Wang, G., Nguyen, A.V., Mitra, S., Joshi, J.B., Jameson, G.J., Evans, G.M., 2016. A review of the mechanisms and models of bubble-particle detachment in froth flotation. Sep. Purif. Technol. 170, 155–172.
Wang, G.C., Ge, L.H., Mitra, S., Evans, G.M., Joshi, J.B., Chen, S.Y., 2018. A review of CFD modelling studies on the flotation process. Miner. Eng. 127, 153–177.
Wang, L.-P., Maxey, M.R., 1993. Settling velocity and concentration distribution of heavy particles in homogeneous isotropic turbulence. J. Fluid Mech. 256, 27–68.
Wang, L.-P., Rosa, B., 2009. A spurious evolution of turbulence originated from round-off error in pseudo-spectral simulation. Comput. Fluids 38, 1943–1949.
Wang, L., Wexler, A.S., Zhou, Y., 2000. Statistical mechanical description and modelling of turbulent collision of inertial particles. J. Fluid Mech. 415, 117–153.
Wang, L.P., Ayala, O., Gao, H., Andersen, C., Mathews, K.L., 2014. Study of forced turbulence and its modulation by finite-size solid particles using the lattice Boltzmann approach. Comput. Math. Appl. 67, 363–380.
Wang, L.P., Ayala, O., Kasprzak, S.E., Grabowski, W.W., 2005. Theoretical formulation of collision rate and collision efficiency of hydrodynamically interacting cloud droplets in turbulent atmosphere. J. Atmos. Sci. 62, 2433–2450.
Wang, W., Zhou, Z., Nandakumar, K., Xu, Z., Masliyah, J.H., 2003. Attachment of individual particles to a stationary air bubble in model systems. Int. J. Miner. Process. 68, 47–69.
Yoon, R., Luttrell, G., 1989. The effect of bubble size on fine particle flotation. Miner. Process. Extractive Metall. Rev. 5, 101–122.
Yoon, R., Luttrell, G., ADEL, G., Trigg, R., 1984. Cleaning of ultrafine coal by microbubble flotation. In: Proceedings of First Annual Pittsburgh Coal Conference. Pittsburgh, Pennsylvania, pp. 880–896.
Zhang, H., Liu, J., Wang, Y., Cao, Y., Ma, Z., Li, X., 2013. Cyclonic-static micro-bubble flotation column. Miner. Eng. 45, 1–3.